Proceedings of the 1998 IEEE/RSJ
Intl. Conference on Intelligent Robots and Systems
Victoria, B.C., Canada • October 1998

Tele-Nanorobotics Using Atomic Force Microscope

Metin Sitti and Hideki Hashimoto
Institute of Industrial Science, University of Tokyo
Roppongi, 7-22-1, Minato-ku, Tokyo, 106-8558, Japan
sitti@vss.iis.u-tokyo.ac.jp
hashimoto@iis.u-tokyo.ac.jp

Abstract

In this paper, a tele-nanorobotics system using Atomic Force Microscope (AFM) as the nanorobot has been proposed. Modeling and control of the AFM cantilever, and modeling of nanometer scale forces have been realized for telemanipulation applications. Besides of 3-D Virtual Reality visual feedback in the user interface, a 1DOF haptic device has been constructed for nano scale haptic sensing. For feeling the nano forces, a bilateral teleoperation control system with Virtual Impedance approach has been introduced. Initial experiments and simulations on AFM and teleoperation system show that the system can be utilized for different tele-nanomanipulation applications such as 2-D nano particle assembly or biological object manipulation.

1 Introduction

Controlled action at a distance, teleoperation, has been used since the earliest times to extend man's reach into hostile or distant places. Telerobotics systems for operating robots in hazardous environments, outer space or deep sea have been a recent hot topic in the field of teleoperation. Besides of these kinds of applications, there is a new emerging application area of such systems which we call *Tele-Nanorobotics*. Since man cannot sense or manipulate directly in the nano scale world, one solution is teleoperation between macro and nano worlds. This kind of application has become possible by the invention of Scanning Tunneling Microscope (STM) and Atomic Force Miscoscope (AFM) which can provide atomic size 3-D topology images. Although the nano scale imaging technologies are being established, nano scale manipulation and fabrication technologies are still in their early infancy. Therefore, the aim of this study is to construct a direct teleoperation system which will enable teleoperated manipulation of nano scale objects with sizes in the range of $1nm - 1\mu m$ by an interdiciplinary research among computer scientists, physicists, chemists, molecular biologists and material scientists. Applications of such a system can be in biological systems such as manipulating cells or genes for repairing or understanding mechanisms more clearly, computer industry such as high-density disk storage and miniaturization of integrated circuit components, semiconductor physics such as hand-made nano devices, and material science such as fabricating man-made materials.

Few existing studies in nanometric scale manipulation can be classified into two main groups: STM-based and AFM-based manipulation systems. STM measures the tunneling current between its metallic probe and sample while scanning in x-y direction. On the other hand, AFM measures the interatomic forces between the AFM tip and sample atoms or force gradient by detecting the cantilever deflection using laser interferometry or other methods while scanning. In both systems, during 3-D topology imaging, z-position of the cantilever or sample is controlled by $0.1nm$ order resolution for helding a pre-set constant effect between the probe and sample.

Comparing these microscopes, in STM, by applying voltage pulses between the probe and sample, manipulation of atoms or molecules [1] in 2-D or 3-D is possible. However, AFM tip can only realize more mechanical tasks such as push and pull of particles on a substrate [2], [3], [4], and the smallest manipulated particle is around 15 nm radius upon our knowledge due to the mechanical difficulties for moving atoms or molecules in the respects of tip size and strong interatomic forces. On the other hand, AFM has more application areas since it is applicable to all materials while STM can be used only for conducting or some semi-conducting materials. Furthermore, STM gives only topology data, but AFM can provide both topology and interaction force data. This point is very advantageous in AFM for reliable force feedback from the nano world to the macro world.

In all of the nano-manipulation studies, manipu-

0-7803-4465-0/98 $10.00 © 1998 IEEE

lation tasks are realized by trial and error or semi-autonomous control approaches. Manipulated object sizes are between atom size and around 10s of nm. From these studies, only one uses teleoperation including force feedback depending upon our information. Falvo et al. [5] utilizes commercial AFM and haptic device for real-time force and 3-D visual feedback. They utilize plane and probe model [6] for surface force feedback, but they do not have any report on teleoperation control problem and force modeling. Furthermore, Hollis et al. [7] constructed a teleoperated atomic scale tactile-feedback system utilizing STM as the slave and 6DOF fine motion device called Magic Wrist as the master device. Their system does not have any force-reflecting behaviour.

This paper discusses a bilateral force feedback teleoperation control system with nano scale force modeling for the nano scale tele-manipulation applications where a 3-D Virtual Reality (VR) visualization interface and 1 DOF haptic master device coupled with a home-made AFM for feeling and manipulating nano scale objects are constructed.

The organization of the paper is as follows: at first, the master device with its model and control, then, AFM as the slave device with its model, principle, and control are explained. Next, the VR system and teleoperation control system with their experimental results are given. Finally, conclusions and future directions are reported.

2 Master/Haptic Device

For feeling the interatomic force normal to the AFM tip (frictional forces are excluded in this study), a 1DOF master device as shown in Figure 1 is constructed [8]. It consists of a linear motor which can be modeled as simple DC motors with the transfer function:

$$C(s) = \frac{X(s)}{E_a(s)} = \frac{K_m K_p}{s(T_m s + 1)} \tag{1}$$

where X is the displacement of the motor shaft, E_a is the applied armature voltage. The parameters and properties of the device is given in Table 1. Using a proportional controller with constant $G = 10000$, the closed loop transfer function becomes as

$$M(s) = \frac{C(s)G}{1 + C(s)G} = \frac{a^2}{s^2 + bs + a^2} \tag{2}$$

where $b = 1/T_m$ and $a^2 = GK_mK_p/T_m$.

Operator puts his/her hand to the master arm, applies the normal force $F_{op}(t)$ to the arm tip, and meanwhile feels the arm motion, $x_m(t)$. There is no power transmission from operator to the master arm; the arm moves by motor control every time in accordance with the operator force.

Bandwidth	$\simeq 30Hz$	*Range*	$20mm$
Friction	$\pm 3.15mNm$	K_p	2.79×10^{-5}
K_m	$29.41(rad/sec)/V$	T_m	$0.0011sec$

Table 1. Properties and parameters of the haptic device.

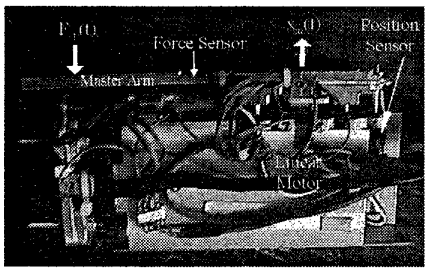

Figure 1: 1DOF haptic device with a linear motor, and force and position sensors.

3 AFM: the Nanorobot and Sensor

A specific AFM cantilever is used for nano imaging and manipulation as can be seen Figure 2. It is a Si cantilever that exhibits piezoresistive effect [9] such that when the cantilever is stressed by any external force, the resistance of the cantilever changes. Thus, using a dc-biased Wheatstone bridge and assuming small deflections, the change of the resistance can be converted into a voltage change such that:

$$\Delta V(t) = 0.25 V_0 G_c S_c \zeta(t), \tag{3}$$

where $t \in R$ is the time, $\Delta V(t)$ is the voltage change in the bridge output voltage, V_0 is the bridge supply voltage, $G_c = 100$ or 10000 is the gain in the amplifier, S_c is the sensitivity of the cantilever to the resistance change per nm, and $\zeta(t)(nm)$ is the cantilever deflection from the rest position. This equation can be used to convert the measured voltage values into nm deflection. S_c is computed experimentally by moving the cantilever with known displacements while the tip is at contact with the sample.

The present system can realize only contact-type of AFM images. However, for the manipulation applications, the nano objects to be manipulated are designed not to be fixed on the subtrate. Therefore, during imaging, contact-type of scanning is undesirable, and non-contact or tapping-type of AFM imaging is required. We prefer tapping-type imaging where soft samples can be scanned with few deformation, and unstabilities due to the surface adhesion forces are less.

Therefore, our strategy is *imaging in the tapping mode and manipulation in the contact-mode.* In the tapping mode, the cantilever tip is set to several 10s of nm above the substrate, and it is vibrated externally around its resonance frequency f_r by an amplitude equal to its separation distance. Thus, the tip taps to the substrate, and the interatomic forces change the vibration amplitude and frequency. Detecting these changes and controlling the sample/cantilever z-position during scanning, surface image is held. This kind of imaging mode will be added to our system.

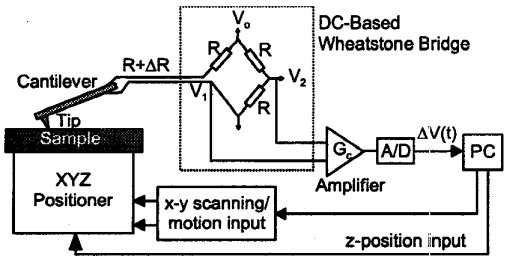

Figure 2: AFM with piezoresistive cantilever and electronic detection system.

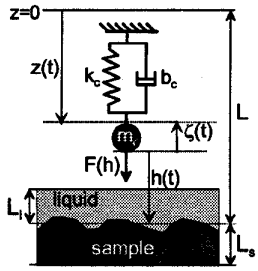

Figure 3: AFM cantilever model as a simple harmonic oscillator.

Modeling of the cantilever and nano force dynamics is essential for reliable manipulation control. Cantilever dynamics can be modeled as a simple mass-spring system as shown in Figure 3 with effective mass $m_c = k_c/(4\pi^2 f_r^2)$, damping $b_c = \pi f_r/Q_c$ (Q_c is the quality factor of the cantilever in air), and stiffness k_c such that during approaching and retracting from a sample surface

$$m_c\ddot{h}(t) + 2m_c b_c(\dot{h}(t) + \dot{z}(t)) + k_c(h(t) + z(t) - L) = \begin{cases} F_{non-con}(h(t)) - B_0^l\dot{h}(t)u(h(t) - L_l), & h(t) > a_0 \\ F_{con}(h(t)) - B_0^s\dot{h}(t), & h(t) \le a_0 \end{cases} \quad (4)$$

where $F_{non-con}(t)$ and $F_{con}(t)$ are the non-contact and contact tip-sample interaction forces, $h(t)$ is the tip-sample distance, $z(t)$ is the tip-position from the initial rest point, L is the tip-sample initial rest distance, $B_0^l \approx \pi\tau_l R_c(a_0 - h(t))/L_l$ is the liquid-layer damping, $B_0^s \approx \pi\tau_s R_c(a_0 - h(t))/L_s$ is the sample damping, R_c is the cantilever tip radius, the function $u(x)$ is equals to 0 if $x < 0$ and to 1 else, τ_l and τ_s are the viscosity constants and L_l and L_s are the thicknesses of the liquid layer and sample respectively, and $a_0 = 30^{-1/6}\sigma$ is the contact point where σ is the interatomic distance. Here, the cantilever deflection $\zeta(t)$ which is the experimentally measured quantity is defined as $\zeta(t) = h(t) + z(t) - L$.

In the non-contact region, main forces are van der Waals, capillary and electrostatic forces such that $F_{non-con}(t) = F_{vdw}(t) + F_{ad}(t) + F_{el}(t)$. Electrostatic forces are excluded in this study, and will be included in next publications. Thus, using Lennard-Jones model, and assuming the interaction of the spherical cantilever tip and a flat surface,

$$F_{non-con}(h(t)) = -F_0\Big(\frac{\sigma^2}{h(t)^2} - \frac{\sigma^8}{30h(t)^8}\Big) + F_{cap}(h(t)). \quad (5)$$

Here, $F_0 = \frac{HR_c}{6\sigma^2}$, and H is the Hamacker constant ($0.4 \times 10^{-19} < H < 5 \times 10^{-19}$ for all materials). For the case of a liquid layer on the sample, $H = \{(H_{tip} - H_{liquid})(H_{sample} - H_{liquid})\}^{1/2}$ [10]. For example, for a SiO_2 tip and mica sample with a water layer on it case, $H \approx 1.89 \times 10^{-19}J$ where $H_{SiO_2} \approx 4 \times 10^{-19}J$, $H_{H_2O} = 0.37 \times 10^{-19}J$ and $H_{mica} = 1.35 \times 10^{-19}$.

For the capillary force, including solid-solid adhesion force $F_{s-s} = 4\pi R_c\gamma_{SL}$, due to the liquid meniscus two equations are needed during approaching and retracting such that

$$\begin{aligned} F_{cap}^{app}(h(t)) &= -\frac{4\pi R_c\gamma_L}{1+\frac{h(t)-a_0}{2r_1}}u(h(t) - 2r_1) - F_{s-s}, \\ F_{cap}^{ret}(h(t)) &= -\frac{4\pi R_c\gamma_L}{1+\frac{-h(t)+\delta}{2r_1}}u(-h(t) + \delta) - F_{s-s}, \end{aligned} \quad (6)$$

where r_1 is the meniscus curvature radius (r_1 can be approximated as $r_1 \approx -0.54/log(P/P_s)(nm)$ using Kelvin equation [10] assuming a water layer at $20C^o$ where P/P_s is the relative humidity ratio), thickness of the water layer is assumed as $L_l \approx 2r_1/3$, δ is the breaking length of the meniscus, γ_L is the liquid surface energy (for water $\gamma_L = 72mJ/m^2$), and γ_{SL} is the surface energy between solid-liquid interface. Often $\gamma_L > \gamma_{SL}$, and the F_{s-s} force can be ignored. As the notation, the (-) force means the attractive and (+) do repulsive forces.

In the contact region, the repulsive elestic deformation/indentation forces with surface adhesion are to be

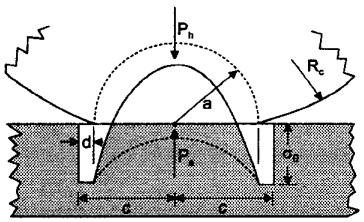

Figure 4: Continuum mechanics model of the elastic contact using Maugis-Dugdale approach.

modeled. Assuming still in the limit of continuum mechanics, Maugis-Dugdale (MD) contact model seems to be the best available analytical model [11] for AFM studies where it enables a transition from the JKR contact model to DMT contact model. MD model assumes a constant stress $\sigma_0 = 1.03/a_0$ over the annulus d in Figure 4. The net contact force is made up of the Hertz pressure P_h and adhesive tension P_a, and given as:

$$\frac{F_{con}(t)}{\pi\omega R_c} = A(t)^3 - \lambda A(t)^2\{\sqrt{m^2-1} + m^2 cos^{-1}(\frac{1}{m})\}. \quad (7)$$

For a maximum stress σ_0, the non-dimensional parameter λ is defines as

$$\lambda = 2\sigma_0\Big(\frac{9R_c}{16\pi\omega E^{*2}}\Big)^{1/3}. \quad (8)$$

where $E^* = ((1-\nu_{tip}^2)/E_{tip}+(1-\nu_{sample}^2)/E_{sample})^{-1}$, E is the Young modulus and ν is the Poisson's coefficient, and ω is the work of adhesion (if water layer exists, $\omega = \gamma_L + \gamma_S - \gamma_{SL}$). Given λ, $m(t) = c(t)/a(t)$ and the normalized contact area $A(t) = a(t)(4E^*/(3\pi\omega R_c^2))^{1/3}$ can be computed by the following equations:

$$\frac{\lambda A(t)^2}{2}[\sqrt{m^2-1} + (m^2-2)cos^{-1}\frac{1}{m} + \frac{4\lambda^2 A(t)}{3}[\sqrt{m^2-1}cos^{-1}\frac{1}{m} - m + 1] = 1, \quad (9)$$

$$\Delta(t) = A(t)^2 - \frac{4\lambda A(t)}{3}\sqrt{m^2-1}, \quad (10)$$

$$\Delta(t) = (L - x_s(t))\frac{9\pi\omega^2 R_c)}{16E^{*2}}. \quad (11)$$

$\Delta(t)$ is the normalized indentation distance. If $\lambda \to 0$, The MD model converges to the DMT model, and if $\lambda \to \infty$ it converges to the JKR model.

For the case of spherical particle and tip interaction, the above force equations are the same with only changes of $\omega \to \gamma_{sl}$ and $R_c \to R_c R_p/(R_c + R_p)$ where R_p is the particle radius. Thus, using these equations, the forces between a particle and a flat substrate, and between the tip and the particle can be computed for controlling the forces during pushing manipulation of particles on a flat substrate for the application of 2-D assembly of particles. But, during pushing or moving the particles on the substrate, the friction force also plays a major role, and its modeling and the control of all forces during pushing are given in [12].

Using the above dynamical models with the parameters listed in Table 2, the approach and retraction of a cantilever tip to a sample surface is simulated. Assuming a slow approach, the dynamics is quasi-static, i.e. $F(h) = k_c\zeta(t)$ where the derivative terms in the Eq. 4 are omitted. Resulting $F(h)$ vs. $h(t)$ curve is shown in Figure 5. The tip contacts with the sample at the point C and leaves it at D during retracting. The hysteresis in the cantilever deflection is due to the energy dissipation. Energy dissipation sources are: (1) *adhesion forces* which cause dissipation if ω is high and k_c is low, (2) *mechanical instabilities* if the cantilever stiffness is smaller than the interaction force gradient, (3) *liquid layer* which causes dissipation as a damper. As the experimental result, force-distance curve is held by approaching to and retracting from a mica sample surface using a cantilever with $k_c = 8N/m$, $R = 2K\Omega$, $G = 10^4$, $V_0 = 2.5V$ and $S_c = 1 \times 10^{-6}/nm$ as can be seen in Figure 6. The electrical and environmental noises can be seen in the figure. The measurements are realized by the home-made AFM shown in Figure 7. in the repulsive region. It can be seen that the $F(h(t))$-$h(t)$ relation is approximately linear in the contact region.

$k_c = 40N/m$	$f_r = 150KHz$	$R_c = 10nm$
$Q_c = 100$	$\gamma_L = 0.073J/m^2$	$H = 1.89 \times 10^{-19}J$
$\omega = 0.072J/m^2$	$E_{tip} = 170GPa$	$E_{sample} = 4GPa$
$\nu_{sample} = 0.3$	$\nu_{tip} = 0.5$	$\sigma = 3.49A^o$
$L_l = 0.8nm$	$r_1 = 1.2nm$	$\delta = 4nm$

Table 2. Parameters of the AFM simulation model.

4 Visualization Interface

Real-time and interactive visual feedback from the nano world which gives information about surface roughness, shape, texture, etc. is essential besides of haptic feedback. Since AFM can measure the 3-D topology, this information can be presented to the user in a friendly way. VR graphics technology has been used for generating sample images in 3-D, and the details of the VR system is given in [13]. An ex-

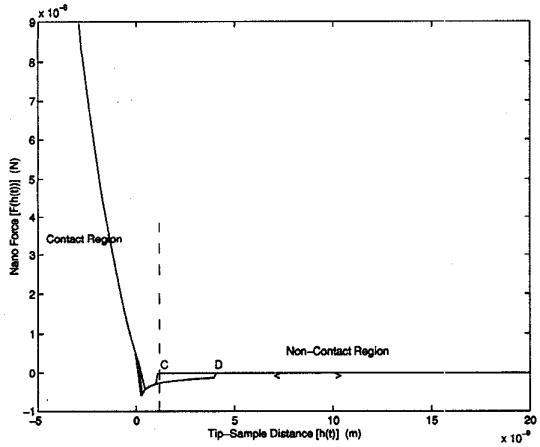

Figure 5: Force-distance relation during approaching and retracting process (simulation).

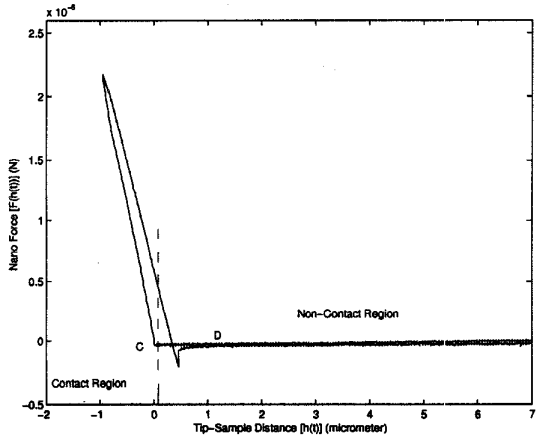

Figure 6: Force-distance relation during approaching to and retracting from a mica sample (experiment).

ample of 3-D images generated using OpenGL software environment is shown in Figure 8. This image can be rotated or zoomed in any direction, and can be presented in 3-D to the user using a stereo glass, or a head mounted display.

5 Haptic Feedback Control

5.1 Main Issues

5.1.1 Scaling Effect

Going from macro to nano world, the main phenomenon is the reduction of the size of objects where the effect of length change is defined as scaling effect. By decreasing the size, inertial force decreases with the power of 4, and spring and damping forces do with the power of 2. However, electrostatic force is not affected by the length scaling, thus it is dominant with respect to other forces. Furthermore, resonant

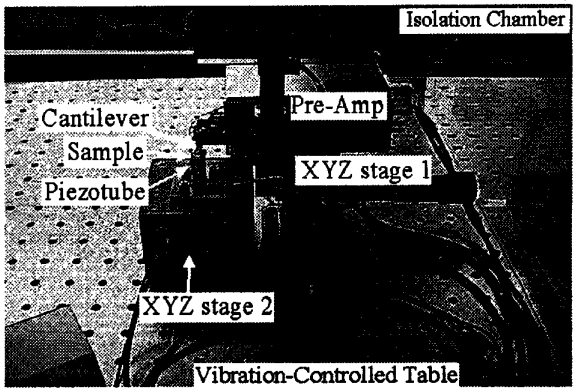

Figure 7: Home-made AFM setup.

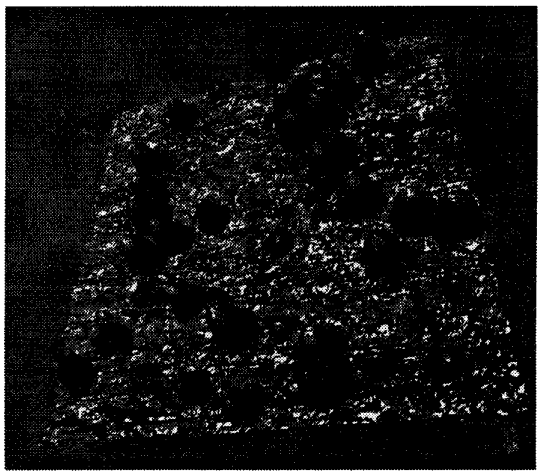

Figure 8: 3-D virtual reality graphics image of InAs dots around 5 nm radius and $10nm$ height with a sample size of $150 \times 150nm^2$.

frequency increases with the length power of 1 which implies that the dynamics in the nano world is very fast. Therefore, quasi-static dynamics approaches are more feasible during the teleoperation control.

For the scaling nano forces and positions to the macro world, there are mainly two approaches: ***linear*** and ***nonlinear*** scaling. In the former,

$$\begin{aligned} x_s^*(t) &= \alpha_p x_s(t), \\ F_s^*(t) &= \alpha_f F_s(t), \end{aligned} \tag{12}$$

where $F_s(t)$ and $x_s(t)$ represent the slave/nano force and position respectively, $F_s^*(t)$ and $x_s^*(t)$ are the scaled values, and α_p and α_f are constant position and force scales respectively. The selection of α_x and α_p depends on the $F_m(t)$ and $x_m(t)$ mechanical and hardware limits. In this type of scaling, all forces are

scaled in the same way such that the inertial forces can not be felt.

In the nonlinear scaling which is also called *impedance* scaling [9], forces are scaled independently such that

$$\begin{aligned} x_s^*(t) &= \alpha_p x_s(t), \\ F_s^*(t) &= \alpha_p^4 m_c \ddot{x}_s + \alpha_p^2 b_c \dot{x}_s + \alpha_p^2 k_c x_s, \end{aligned} \quad (13)$$

In this approach, the inertial forces can be magnified such that the operator can feel close to its daily experience. But this approach requires precise environment parameters while the linear scaling does not.

5.1.2 Bandwidth Effect

If the relative difference between the bandwidths of the force feedback device, f_m, and slave device, f_s, is high, strategies should be introduced for avoiding unstabilities and unreliable force feeling. In the AFM system, x-y scanning bandwidth is around 50 Hz in closed-loop or around 200 Hz in the open-loop while the force feedback device bandwidth is around 30 Hz without any dedicated hardware. Then, one solution is limiting the scanning speed, $v_s(t)$, for feeling the nanometric/atomic features with length ΔL within the haptic device's bandwidth such that

$$v_s(t) \leq \Delta L f_m. \quad (14)$$

In the reverse case, where $f_m > f_s$, smoothing strategy such as adding artificial compliancy for intermediate motions can be a solution.

5.1.3 Hardware Disturbances

The main hardware disturbance sources in an AFM-based tele-nanorobotic system can be classified depending on the system part such as AFM, master device and teleoperation system disturbations. In the AFM system, mechanical vibration in the range of 1 Hz-10 KHz, hysteresis and thermal drift in the piezoelectric positioners, thermal electrical and $1/f$ noise in the piezoresistive AFM cantilever, water layer due to the humidity in the air, air flow, acoustic pressure, and temperature changes are the main disturbation sources. For reducing acustic and air flow disturbances, an acrylic chamber is designed with double glasses, and a vibration-controlled table is being used in our system. In the haptic device, backlash, sensor error, hysteresis and electrical noises can exist. Additional low-pass filters can reduce the electrical noise. Finally, during teleoperation, time delay can be a significant disturbance especially in distant application cases using the computer network.

5.2 Operation Modes

5.2.1 Tactile Feedback Mode

In this mode, the measured interatomic forces are felt on the operator's hand while scanning a sample such as in [7]. The control method is shown in Figure 9. At first, the cantilever tip is approached to the surface, and put in contact with the substrate. Then, by controlling the x-y motion by a mouse, the operator, putting his/her finger on the haptic device, can feel the relative height of the surface by the position control of the device. Here $\zeta(t)$ is assumed to be directly proportional to the surface height. As the experimental result, an image given in Figure 10 is scanned along the line shown in the figure. The resulting tactile-sensing with the scale parameter $\alpha_p = 0.1cm/nm$ is given in Figure ??. The upward jumps stand for the InAs dots. In this mode, the nano objects are assumed to be fixed on the substrate.

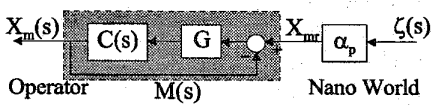

Figure 9: Tactile feedback control.

5.2.2 Bilateral-Force Feedback/Manipulation Mode

In the manipulation mode, during approaching and contacting to the surface or the object, or manipulating the object, the operator controls the x-y-z motion of the cantilever/sample while feeling the normal tip-sample interaction force. Using linear scaling approach, the ideal response of the bilateral teleoperation system is defined as: at the steady-state

$$\begin{aligned} F_m &\rightarrow \alpha_f F_s, \\ x_s &\rightarrow \alpha_p x_m, \end{aligned} \quad (15)$$

where $F_m(t)$ and $x_m(t)$ are the master force and position respectively. $x_s(t) = z(t)$ in the AFM system.

In order to realize the ideal response, the bilateral teleoperation system in Figure 11 is proposed. Virtual Impedance (VI) control approach is utilized to control the impedance between the master and slave arms for realizing the desired force feedback depending on the task. Thus, VI control transfer function term $V(s) = 1/(M_v s^2 + B_v s + K_v)$ generates smooth reference master and slave positions as $x_{mr} = x_{sr}/\alpha_p$ since it also behaves as a second order low-pass filter. $M(s) = X_m(s)/X_{mr}(s)$ (given by the Eq. (2)) and $S(s) = X_s(s)/X_{sr}(s)$ are master and slave plant and control transfer functions. K_f is the force error feedback gain. For the simplicity of the analysis, if a spring is assumed to be attached to the cantilever, i.e.

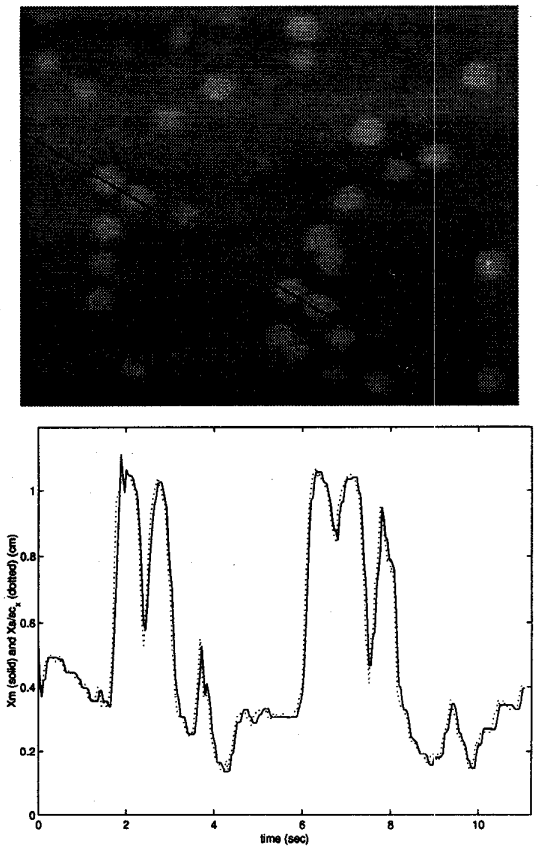

Figure 10: InAs quantum dots are scanned along the black line, and the resulting tactile feedback ($x_m(t)$:solid and $\alpha_p x_s(t)$:dashed lines).

$F_s(s) = KX_s(s)$, following equations are computed for checking the ideal responses:

$$\frac{X_m(s)}{X_s(s)} = \frac{a^2}{\alpha_p(s^2+bs+a^2)S(s)}, \quad (16)$$

$$\frac{F_m(s)}{F_s(s)} = \frac{M_v s^2 + B_v s + K_v}{\alpha_p K K_f} + \alpha_f\left(1+\frac{1}{K_f}\right) \quad (17)$$

In the AFM system, the actuator for the slave cantilever is a piezoelectric positioner which is controlled in open-loop, and it can be assumed that $X_s(s) = X_{sr}(s)$, i.e. $S(s) = 1$, for the simplicity neglecting the nonlinearity and hyteresis problems. Driving the nonlinear modeling and control of the piezo positioner is a future work. Then, the ideal response of $x_s \to \alpha_p x_m$ is held at the steady state by eliminating the differential terms in teh Eq. (16). For the ideal force response, if $K_v = 0$, and $K_f >> 1$, $F_m \to \alpha_f F_s$ as $t \to \infty$. Furthermore, assuming bounded $F_m(t)$ and $F_s(t)$ and providing the ideal responses, the system stability is also held. However, the above analysis is only realized for a spring in the slave site where the nano force $F_s(t)$ is a nonlinear function of $x_s(t)$. Only, in the contact region, $F_s(t) \approx c_1 x_s(t) + c_2$ can be approximated in the range of the elastic deformation interaction where c_1 and c_2 are experimentally fitted constants.

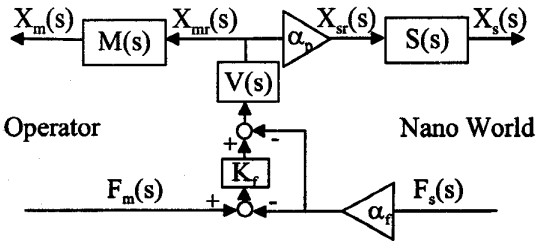

Figure 11: Bilateral force feedback control.

Experimental results of bilateral interaction during approaching to a surface is shown in Figure 12. $M_v = 0.1kg$, $B_v = 20N/(m/sec)$, $K_v = 0$, $\alpha_p = 15 \times 10^{-9}$, $\alpha_f = 1 \times 10^8$, and $K_f = 20$ are taken. Initial tip-sample position is $10nm$. AFM force feedback is simulated using the derived models with the parameters in Table 2. As can be seen in the force-time graph, the operator starts to apply force at around 0.8 sec. Then the master device also begins to move in according to $V(s)$ until to the contact point. After the contact, the point after the (-) nano force, ideal response is being held where $F_m(t)$ and $\alpha_f F_s(t)$ are balanced, and $x_m(t)$ stops. But, if the operator continues to push more, again the controller tracks both forces and positions. When $F_m(t) = 0$ at around 4.6 sec, i.e. operator removes his finger from the device, master device moves back to the contact point again.

6 Conclusion

In this paper, a tele-nanorobotics system using AFM as the nanorobot is introduced. Modeling and control of AFM cantilever, and modeling of nano scale forces have been proposed for telemanipulation applications. Besides of 3-D visual feedback in the user interface, a 1DOF haptic device has been constructed for nano scale tactile sensing and generating motion commands for the AFM. Introducing teleoperation control system with Virtual Impedance approach, nano scale forces or geometries are felt by the operator. Preliminary experiments and simulations on AFM and teleoperation system show that the system can be utilized for tele-nanomanipulation experiments.

Extensions to this system are constructing a 3DOF haptic device with also lateral force feedback, adding friction and electrostatic force models to the AFM

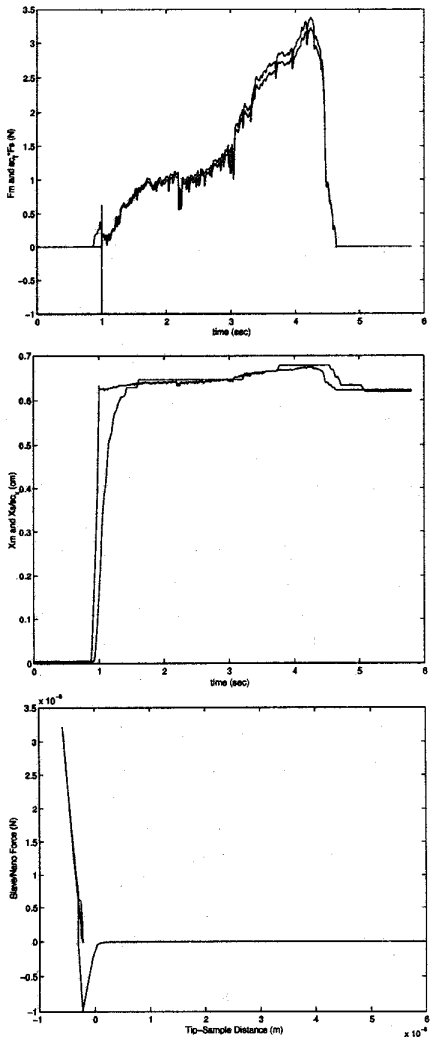

Figure 12: $F_m(t)$ and $\alpha_f F_s(t)$ (upper), $x_{mr}(t)$ and $x_m(t)$ (middle), and $F_s(h(t))$-$h(t)$ (bottom) graphs during approaching and contacting to a mica surface.

force model, and adding delay term to the control loop.

The first goal application is 2-D assembly of nano particles on a flat surface by push and pull operations for understanding the chemical, electrical and mechanical properties of specific materials, and construction of nano devices. The other possible application is biological object such as protein, cell, gene or DNA manipulation.

Acknowledgements

The authors would like to thank PSI Co. for providing piezoresistive cantilevers, and all other Hashimoto Lab. members for their various helps.

References

[1] J. Stroscio and D. Eigler, "Atomic and molecular manipulation with the scanning tunneling microscope," *Science*, vol. 254, pp. 1319–1326, Nov. 1991.

[2] D. Schafer, R. Reifenberger, A. Patil, and R. Andres, "Fabrication of two-dimensional arrays of nanometric-size clusters with the atomic force microscopy," *App. Physics Letters*, vol. 66, pp. 1012–1014, Feb. 1995.

[3] T. Junno, K. Deppert, L. Montelius, and L. Samuelson, "Controlled manipulation of nanoparticles with an atomic force microscopy," *App. Physics Letters*, vol. 66, pp. 3627–3629, June 1995.

[4] T. R. Ramachandran, A. Madhukar, P. Chen, and B. E. Koel, "Imaging and direct manipulation of nanoscale three-dimensional features using the non-contact atomic force microscope," *J. Vac. Sci. Technol. B*, 1997.

[5] M. Falvo, R. Superfine, S. Washburn, and et al., "The nanomanipulator: A teleoperator for manipulating materials at the nanometer scale," in *Proc. of the Int. Symp. on the Science and Technology of Atomically Engineered Materials*, pp. 579–586, Nov 1995.

[6] W. R. Mark, S. C. Randolph, M. Finch, and et al., "Adding force feedback to graphics systems: Issues and solutions," in *Computer Graphics Proceedings SIGGRAPH*, pp. 447–452, 1996.

[7] R. L. Hollis, S. Salcudean, and D. W. Abraham, "Toward a tele-nanorobotic manipulation system with atomic scale force feedback and motion resolution," in *IEEE Int. Conf. on MicroElectromechanical Systems*, pp. 115–119, 1990.

[8] H. Hashimoto and S. Monorotkul, "Tele-handshake through the internet," in *IEEE Int. Workshop on Robot and Human Communication*, pp. 90–95, 1996.

[9] J. E. Colgate, "Robust impedance shaping telemanipulation," *IEEE Transactions on Robotics and Automation*, vol. 9, pp. 374–384, Aug. 1993.

[10] J. Israelachvili, *Intermolecular and Surface Forces*. Academic Press, 1992.

[11] K. Johnson, "A continuum mechanics model of adhesion and friction in a single asperity contact," *Micro/Nanotribology and its Applications, Kluwer Ac. Pub.*, pp. 151–168, 1997.

[12] M. Sitti and H. Hashimoto, "Macro to nano telemanipulation through nanoelectromechanical systems," in *IEEE Ind. Electronics Conf.*, (to be published) Germany, Sept. 1998.

[13] M. Sitti, S. Horiguchi, and H. Hashimoto, "Nano telemanipulation using virtual reality interface," in *IEEE Int. Symp. on Industrial Electronics*, (to be published) South Africa, July 1998.